Electronic Supplementary Material (ESI) for Materials Horizons.

Supporting Information

Highly Sensitive Airflow Sensors with Ultrathin Reduced Graphene Oxide Film Inspired by Gas Exfoliation of Graphite Oxide

ZeyangXu,[a,b]Kunjie Wu[a]SunaZhang,[a]YanchengMeng,[a,b]HongweiLi,[a] and LiqiangLi,[a,*]

Table of Contents:

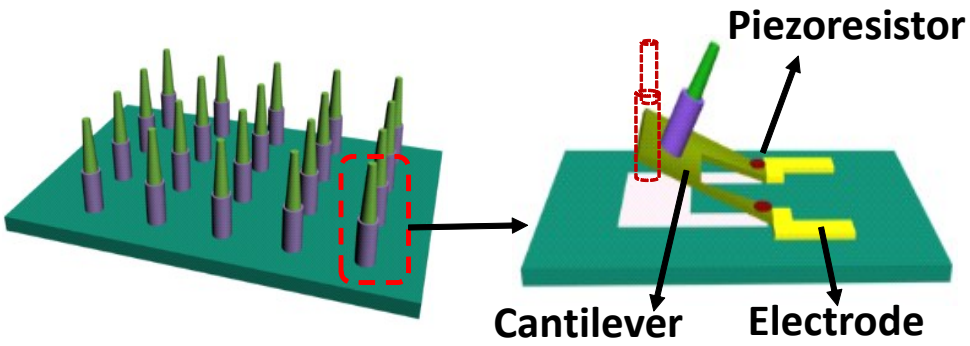

Figure S1 Schematic diagraph of hair airflow sensors based on piezoresistor effect (*Smart Mater. Struc*t. 2012, *21*, 113001).

In the conventional airflow sensors based on mechanical principle, the sensing components may form mechanical deformation due to the airflow. In order to detect the mechanical deformation, the piezoresistive, capacitive, optical, or magnetic effect is adopted. For example, in hair airflow sensor based on Piezoresistive effect (Figure S1a), one Piezoresistor is connected with the artificial hair. The movement of hair due to the airflow may induce the change of resistance of Piezoresistor, which serves as the sensor signal (*Smart Mater. Struc*t. 2012, *21*, 113001). In this airflow sensor, minimization of the diameter is an efficient way to improve the sensing performance, but it poses an technological difficulty for the device fabrications.

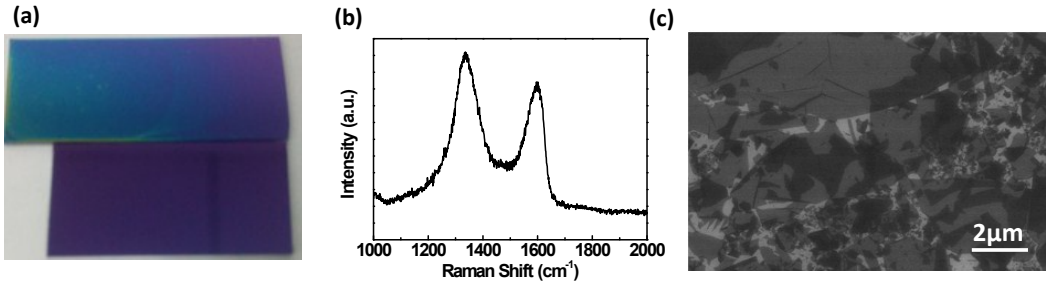

Figure S2(a) Optical images of RGO film prepared via drop-casting (upper part) and covalent-assembly (lower part). (b) Raman spectra of covalent-assembled RGO film. (c) SEM images of covalent-assembled RGO film.

From Figure S2a, it is clear the the covalent assembly method produces more uniform RGO film compared to drop-casting method.

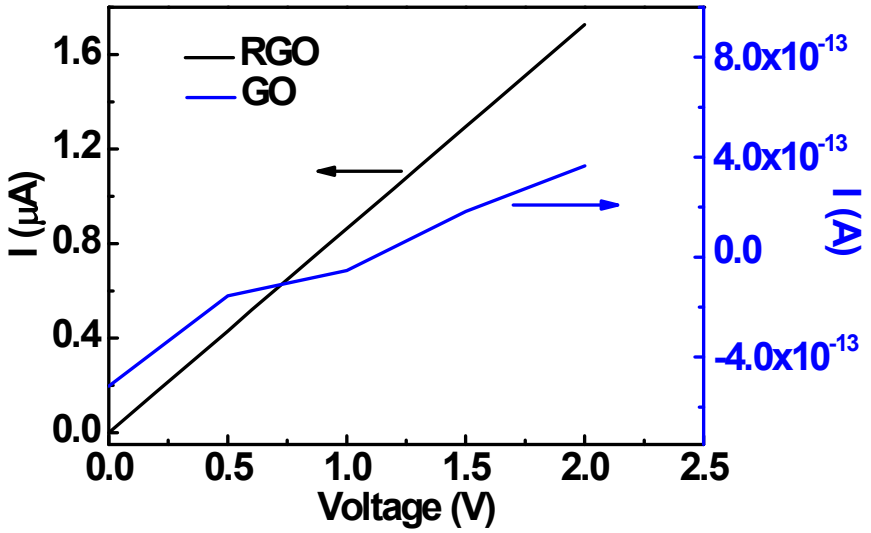

Figure S3 Electrical I-V curves of GO film before and after thermal reduction.

The as-fabricated GO is insulating with current of 10^{-13} A at the voltage of 2 V. After reduction, the current increases over 7 orders of magnitude to 10^{-6} A under the same voltage, indicating the effect of reduction.

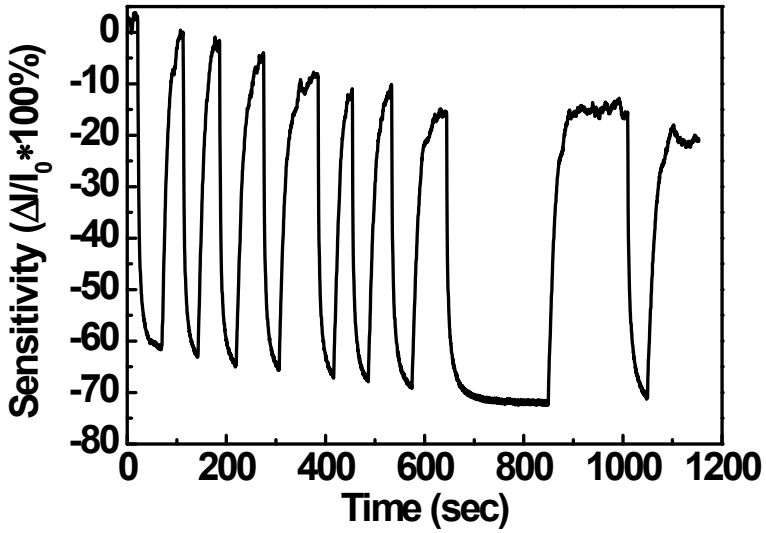

Figure S4 Sensing curve with higher sensitivity of about 60 %.

Occasionally, very high sensitivity of about 60 % can be obtained on the RGO sensor, but the reproducibility is low. Generally the sensitivity is in the range of 32-45 %. The higher sensitivity implies the potential for further improvement.

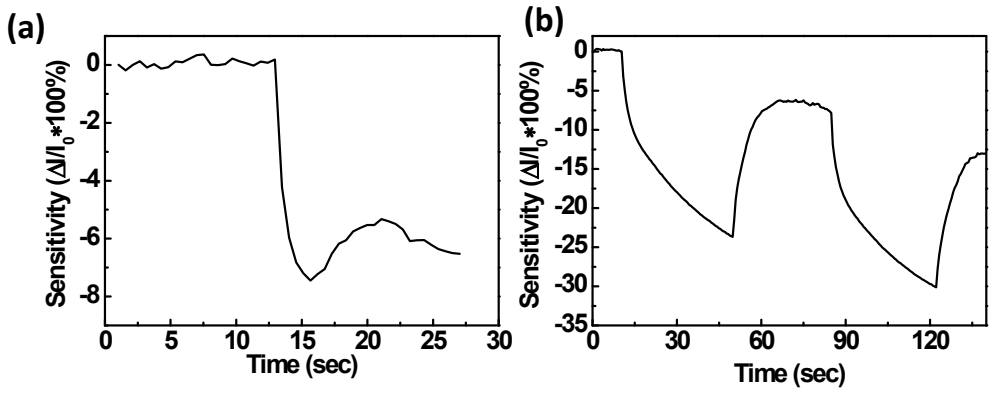

Figure S5 Airflow sensing curves of (a) ~ 10 nm and (b) ~ 4 nm RGO film prepared via drop-casting method.

10 nm RGO film via drop-casting show clear response to airflow, but the recovery is very weak. In contrast, 4 nm RGO film shows better response and recovery. However, 4 nm RGO film is not continuous over large area, which result in big problems in device fabrication. We have tried to fabricate device arrays in about 4 nm RGO region, but the success percent is lower than 20 %. This fact implies the ultrathin film prepared via physically assembly is not suitable for large-area and mass production.

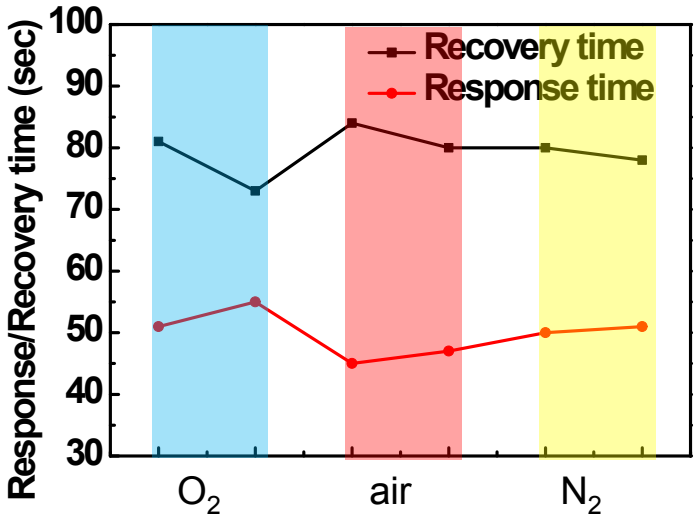

Figure S6 the response and recovery time of RGO sensor toward different gases at the airflow velocity of 1.5 m/s.

Generally, the response/recovery rate of most of sensors is relatively quick at the beginning state, and then gradually becomes slow due to the saturation effect. Accordingly, the response/recovery time is not defined as the whole period from the

gas on/off to gas off/on. It is always defined as the period from the gas on/off to the point that reaches certain sensitivity (i.e., $(I-I_0)/I_0*100\%$), which represents the quick response or recovery period. Therefore, when discussing the response/recovery time, it is necessary to provide the sensitivity which is used to define the response/recovery time. Furthermore, it is known that the sensitivity is related to the airflow velocity, so it would be more precise to provide the airflow velocity. With the airflow velocity and sensitivity, the extracted response/recovery time in different experiments may be comparable. Base on this consideration, in Fig. 4a, the response/recovery time is defined as the period which produces a sensitivity ($(I-I_0)/I_0$) × 100 %) of 25 %. The averaged response time for O_2, air, N_2 are 54, 46, and 51 s, respectively, and the corresponding recovery time are 77, 82, and 79 s, respectively. The sensitivity used for extract response/recovery time and airflow velocity used for test are 25 % and 1.5 m/s, respectively. The extracted response/recovery data indicate the response/recovery time is similar at the same sensitivity for the different gas. The small difference may be due to the experimental errors or the different adsorption ability of gas on RGO surface.

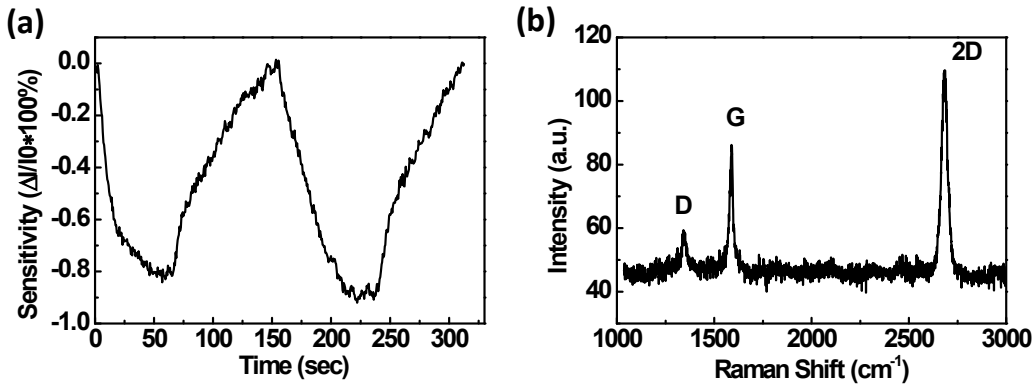

Figure S7(a) Airflow sensing curve of graphene grown via CVD method. (b) Raman spectra of graphene.

The monolayer graphene with some defects confirmed by Raman spectra (Figure S7b) shows very weak sensitivity to airflow (Figure S7a). The removal of H_2O adsorbed on the surface of graphene may mainly account for this behavior.

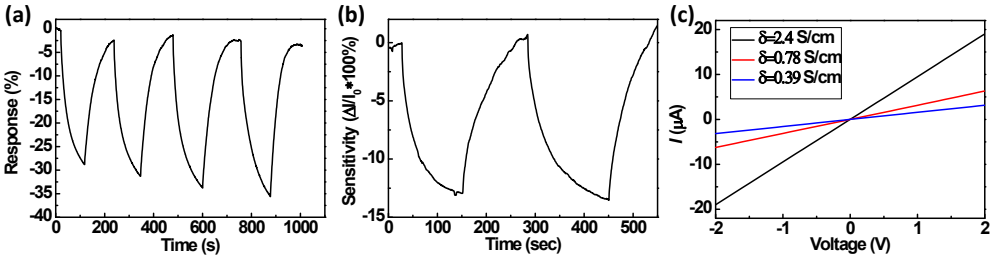

Figure S8(a) Sensing curve of RGO film with conductivity of 0.78 S/cm. (b) Sensing curve of RGO

film with conductivity of 2.4 S/cm. (c) Electrical *I-V* curves of RGO film with different conductivity.

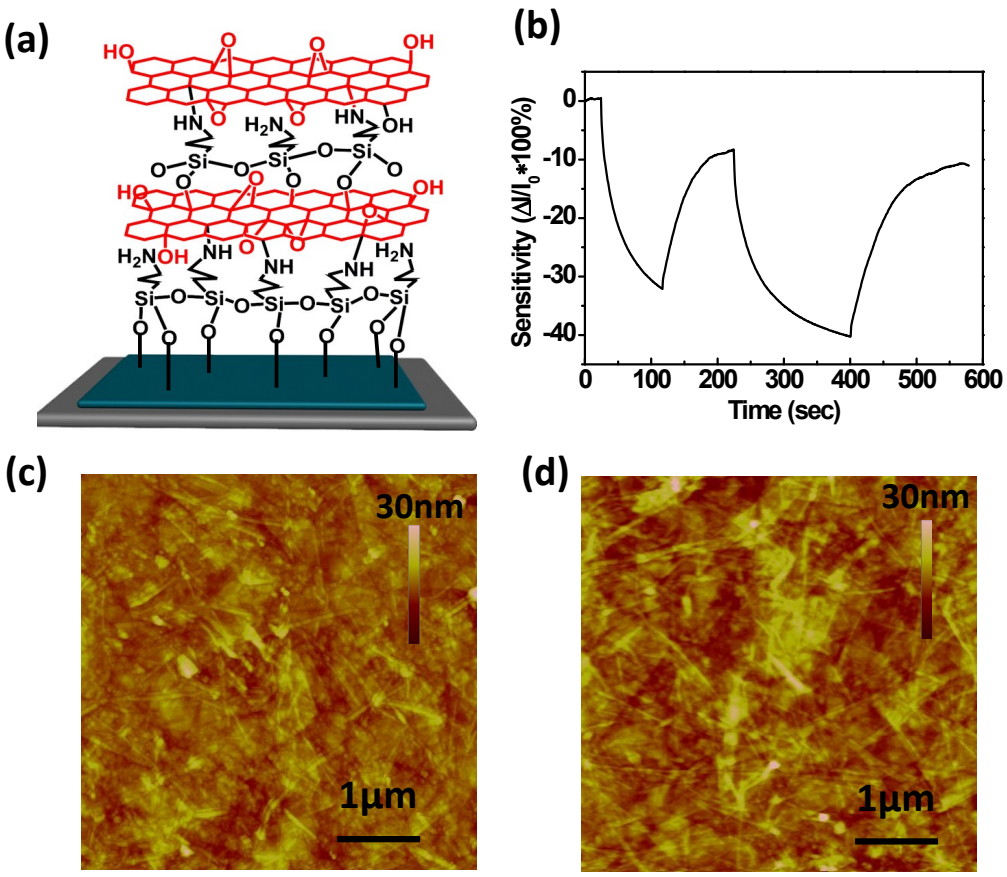

Figure S9(a) Schematic illustration of multilayer GO film prepared via layer-by-layer covalent assembly method. (b) Sensing curve of RGO film with nominal 4 layers. (c) AFM image of RGO film with 4 layers. (d) AFM image of RGO film with 10 layers.

Figure S9a displays the molecular structure of multilayer RGO film prepared via layer-by-layer covalent assembly. Figure S9c,d are the image of 4 and 10 layers RGO film. It should be notes that the layer number denote the assembly times of GO rather than the real number of GO sheets. From AFM images, the GO sheets could not be identified because the surface roughness is greatly larger than the thickness of GO sheets.

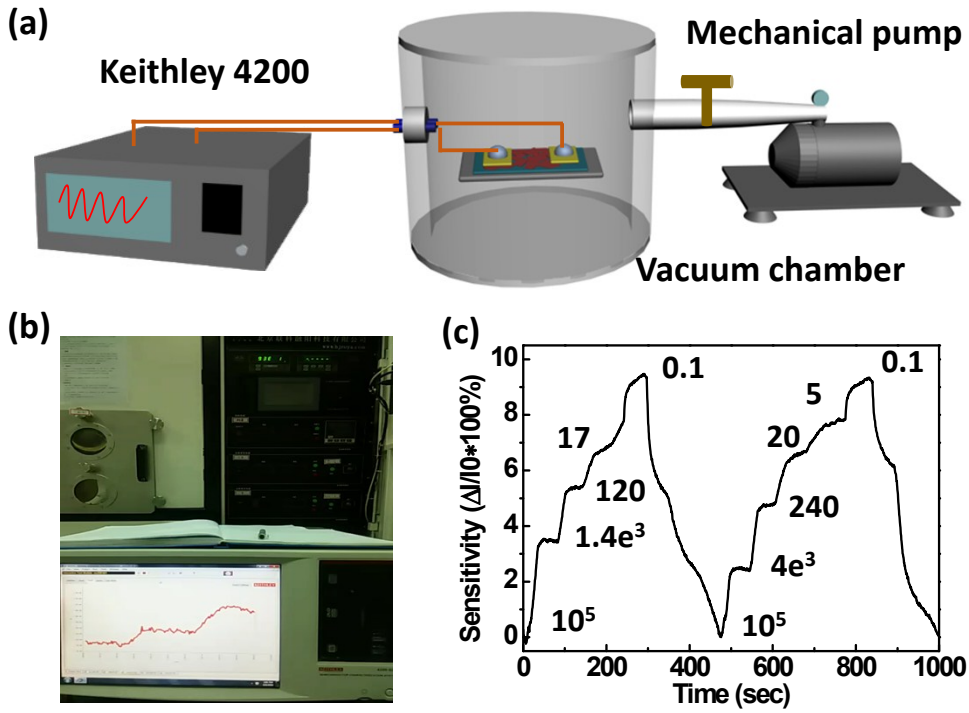

Figur

e S10(a) Schematic diagraph of setup for the vacuum sensor. (b)Experimental setup for the vacuum sensor test. (c) two-cycles vacuum sensing curves. The numbers in c represent the vacuum pressure with unit of Pa.

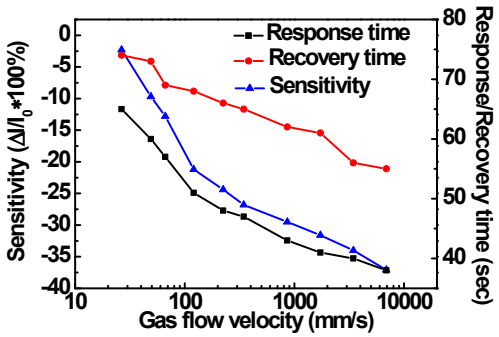

Figure S11. Respnse/recovery time of RGO sensor under various airflow velocity.

As stated in Figure S6, the response/recovery time should be defined at the certain sensitivity, so Figure S11 provide response/recovery time and the sensitivity which are used to define those time values. It can be clearly seen that the response/recovery time decrease with the increasing airflow velocity.